FINITE ELEMENT SIMULATION OF THE FRACTURE BEHAVIOUR OF ELASTOMERS WITHIN A LARGE TRANSFORMATION FRAMEWORK

S. Thuillier and G. Rio[1]

Finite element simulation of the behaviour of a pre-cracked elastomer body is performed, in order to characterize the influence of non-linearities (kinematics and constitutive law) on the stress distribution in the vicinity of the crack tip. The general framework of the modelling is large geometric transformations, including large deformations, and the constitutive behaviour of the material is of hyperelastic type.
The results show the evolution of the invariants of the stress tensor with the distance ahead of the crack tip r. A variation of the kind $r^{-\alpha}$ is discussed, where α depends on the material parameters.

INTRODUCTION

The field of fracture mechanics has been widely investigated using the small deformation assumption and a linear elastic constitutive law. Such assumptions lead to a stress field near the crack tip singular in $r^{-1/2}$, where r is the distance ahead of the crack. The study of these singularities leads to the definition of the stress intensity factors, e.g. K_I in mode I. The stress and strain field analysis in the vicinity of the crack is therefore a basis to understand the behaviour of a cracked component (Lemaitre and Chaboche (1)). When an elastomer is deformed in a quasi-reversible way up to very large strains, it has to correspond physically to a non-linear behaviour; the assumptions underlying linear fracture mechanics are then no longer relevant. Though recent studies deal with fracture mechanics in the case of large displacements-small deformations, e.g. Mialon and Visse (2), the field of non-linear fracture is still under current investigation when non-linearities arise both from kinematics and constitutive behaviour.

A finite element simulation of the behaviour of a pre-cracked body is presented in this paper. Calculations are performed using a finite element program HEREZH developed at the LG2M. The general framework of the modelling is large geometric

[1]Laboratoire de Génie Mécanique et Matériaux (LG2M) - Université de Bretagne Sud - Centre de Génie Industriel - Guidel-Plages 56520 Guidel (France)

transformations, including large deformations and the constitutive law is hyperelastic (Favier (3)). Such a law has been used successfully to model the mechanical behaviour during loading of elastomers (Favier et al (4)). After a short overview of the finite element simulation, cf. Rio et al (5) for more details, calculations of the stress and strain fields in a pre-cracked rectangular body under plane strain conditions are presented. Special emphasis is given to the evolution of the stress tensor invariants with r, in an attempt to fit their evolution with a $r^{-\alpha}$ function (α being a positive scalar).

FINITE ELEMENT SIMULATION

Main features of the modelling. Let us consider the evolution between times t and $t+\Delta t$, i.e. between an initial and a deformed state respectively, of a body Ω. Deformation of Ω depends only of the body itself, whatever its position in space. Therefore, a material frame attached to the body is chosen and a curvilinear coordinate system is introduced. For the sake of simplicity, the finite element mesh is chosen as the material frame. The Almansi strain tensor is defined from the metric tensor at $t+\Delta t$, $\boldsymbol{G}$ and the metric tensor at time t convected at $t+\Delta t$ using a two time covariant transport, ${}^{t+\Delta t}_{t}\boldsymbol{G}$: ${}^{t+\Delta t}_{t}\boldsymbol{\varepsilon} = \frac{1}{2}(\boldsymbol{G} - {}^{t+\Delta t}_{t}\boldsymbol{G}) \overset{noted}{=} \boldsymbol{\varepsilon}$. Equilibrium equations are approached by the principle of virtual power in weak formulation and the final non-linear system is solved by a Newton-Raphson method.

Constitutive behaviour. The general definition is made from a reference state and relies on the assumption of an elastic energy which is a state function. The Cauchy stress tensor $\boldsymbol{\sigma}$ is defined from the scalar elastic energy density $\mathcal{E}$ (eq. (1)) where $\boldsymbol{D}$ denotes the strain rate tensor and $g = |G_{ij}|$. Indeed, $\mathcal{E}$ depends on scalar variables p_α (eq. (2)) which characterize the geometric evolution of the body between the reference state and the deformed state (eq. (3)).

$$\frac{\partial \mathcal{E}}{\partial t} = \sigma^{ij} D_{ji} \frac{1}{\sqrt{g}} \quad (1) \qquad \frac{\partial \mathcal{E}}{\partial t} = \frac{\partial \mathcal{E}}{\partial p_\alpha} \frac{dp_\alpha}{dt} \quad (2) \qquad \frac{dp_\alpha}{dt} = f_\alpha^{ij} D_{ji} \quad (3)$$

For an isotropic material having a symmetric tensile-compression behaviour, the variables p_α can be related to the first and second invariants of the strain tensor, i.e. the volume variation v and $\overline{II}_{\bar{\varepsilon}} = \frac{1}{2}\,\bar{\varepsilon}^{i}{}_{j}\,\bar{\varepsilon}^{j}{}_{i}$. The following dependence has been used in the calculations:

$$\frac{\mathcal{E}}{\sqrt{g}} = \frac{k}{6}(\log v)^2 + \frac{Q_o^2}{2\mu_r}\left[\ln\left(\cosh\left(\frac{2\mu_r}{Q_o}\sqrt{2\overline{II}_{\bar{\varepsilon}}}\right)\right)\right] + \mu_\infty \overline{II}_{\bar{\varepsilon}}$$

where k is an incompressibility modulus and μ_r, Q_o and μ_∞ are defined in Fig. 1.

NUMERICAL RESULTS

Tensile test

The order of magnitude of the material parameters are chosen to be consistent with the behaviour of an elastomer. Fig. 2 shows the stress-strain curve of a simulated tensile test. The corresponding numerical values are presented in table 1.

LINEAR ELASTIC	Young modulus $E = 9.0$		Poisson ratio $\nu = 0.45$	
HYPERELASTIC	$k = 30.0$	$\mu_\infty = 1.0$	$\mu_r = 2.0$	$Q_o = 0.2$

TABLE 1 - Numerical values (in MPa) of the material parameters for linear elastic and hyperelastic constitutive laws.

Behaviour of a pre-cracked body

A rectangular pre-cracked body (Fig. 3) is deformed in uniaxial tension in plane strain conditions. The following dimensions are used: length = 800 mm, width = 500 mm, thickness = 5 mm, crack length a = 35 mm. The mesh consists of 695 linear pentaedrons and is made finer near the crack, i.e. in this area the nodes are distributed according to a geometric progression. The characteristic length of the nearest element to the crack tip is around $3.5\,10^{-5} \times a$ which is a right order of magnitude when such a method is used (1). There is only one layer of elements in the thickness.

Validation. In a first step, calculations using a linear elastic constitutive law are performed in order to validate the mesh. The simulated results lead to the knowledge of σ^{22} ahead of the crack and to the displacements u_2 of the border of the crack; the index 2 refers to the direction of the applied stress σ_a. The stress intensity factor K_I is then given by (1):

$$K_I = \underbrace{\lim_{r\to 0} \left(\sigma^{22}\sqrt{2\,\pi\,r}\right)}_{\text{(a)}} = \underbrace{\lim_{r\to 0} \left(\frac{E}{2\,(1-\nu^2)}\sqrt{\frac{2\,\pi}{r}}\,u_2\right)}_{\text{(b)}}$$

Fig. 4 shows the results as well as the analytical solution corresponding to such a geometry, $K_I = 1.122\,\sigma_a\,\sqrt{\pi\,a}$ (c). At low applied stress ($\sigma_a \leq 0.005$ MPa), the product $\sigma^{22}\,r^{1/2}$ tends towards a constant from $r = 0.01$ mm from the crack tip. This distance increases with σ_a, e.g. $r = 0.05$ mm when $\sigma_a = 0.02$ MPa. The shape of the curve indicates that if σ^{22} follows a $r^{-\alpha}$ variation, α must be different from 0.5, even in the elastic case.

Hyperelastic body. The remote applied stress varies up to 0.4 MPa. Above this value some of the elements in the vicinity of the crack become too highly distorted to give reliable results and it also leads to numerical instabilities. Strains reached at the crack tip lie fully within the field of large deformations, e.g. $\varepsilon_{11} = -3.0$ and $\varepsilon_{22} = 0.4$ when $\sigma_a = 0.2$ MPa. A remeshing technique at the crack tip could push further this limitation and is under current investigation.

It is chosen to represent the stress state at a given point of the body by the three invariants of the stress tensor $\boldsymbol{\sigma}$. Only the second one $\overline{II}_\sigma = \frac{1}{2}\,\sigma^i{}_j\,\sigma^j{}_i$ is presented for the evolution of the three of them are very similar. Fig. 5 shows the variation

of $\ln(\overline{II}_\sigma^{1/2})$ with $\ln(r)$. Out of the several calculations performed, it comes that three main areas can be distinguished, each one being associated to a quasi-linear evolution: area I corresponds to a linear elastic behaviour with a slope around -0.5; area II occurs at each applied stress levels with a constant slope and when the stress and strain concentrations are high enough at the crack tip, area III develops with a slope around -0.67. The variation of $\ln(\overline{II}_\varepsilon^{1/2})$ with $\ln(r)$ shows a reverse tendency, i.e. a slope around -0.72 is noted immediately after the elastic area and it decreases in absolute value when getting closer to the crack tip (Fig. 6).

Calculations were performed to study the influence of the material parameters: $0.5 \leq \mu_r \leq 50$, $1 \leq \mu_\infty \leq 50$, $0.01 \leq Q_o \leq 1$, the parameter k being calculated to keep a constant Poisson ratio of 0.45. As a summary, it can be said that:

1. The simultaneous existence of the three areas depends on the stress and strain concentrations at the crack tip, which depend both on the applied stress and the global stiffness of the body. For example, when $\mu_r = 50$ MPa, the body can be submitted to $\sigma_a = 0.4$ MPa and area III develops only above $\sigma_a = 0.2$ MPa (Fig. 7).
2. It seems that whatever the material parameters and the applied stress, area III is characterized by a constant slope of the order of -0.67. This remark should be deepen for higher stress and strain concentrations.
3. The slope of area II depends on the material parameters, see Table 2.

μ_r (MPa)	0.5	2	5	50
slope	×	-0.43	-0.39	-0.27

TABLE 2 - Variation of the slope in area II with μ_r. $\mu_\infty = 1$ MPa, $Q_o = 0.2$ MPa, $30 \leq k \leq 510$.

Conclusion. Although the constitutive law is non-linear, a dependence of the stress components in the vicinity of the crack tip in $r^{-\alpha}$ can still be found, where α depends on the material parameters and on the stress and strain concentrations. It seems that when these concentrations are high, α tends towards -0.67. The strain components show a reverse tendency.

REFERENCES

(1) Lemaitre, J. and Chaboche, J.L., "Mécanique des matériaux solides - chapter 8: Fissuration", Dunod (1985).

(2) Mialon, P. and Visse, E., Proc. 2ème coll. nat. calcul structures, Giens (France), pp. 89-94, 1995.

(3) Favier, D., thèse d'Etat, INPG, Grenoble (France), 1988.

(4) Favier, D., Rio, G. and Manach, P.Y., Proc. coll. int. franc. génie méca. caout. élast. thermoplas., Nancy (France), 1994.

(5) Rio, G., Manach, P.Y. and Favier, D., Arch. Mech., Vol 47, pp. 537-556, 1995.

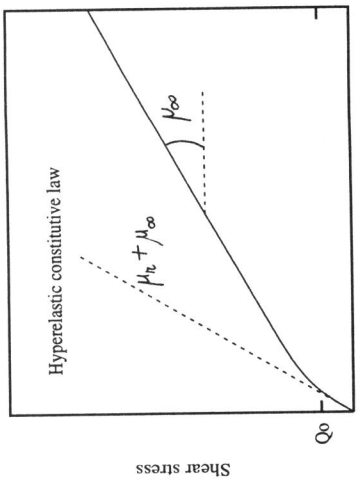

Figure 1: Identification of the material parameters from a shear test.

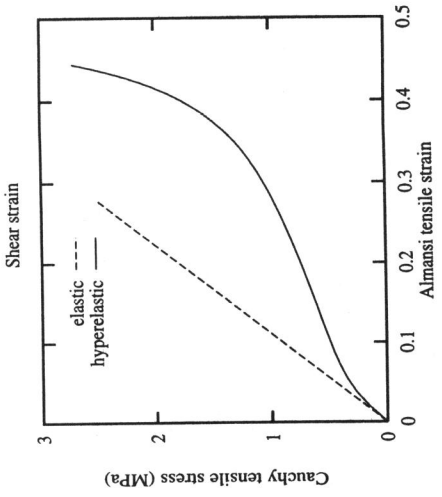

Figure 2: Stress-strain curve recorded during a simulated tensile test.

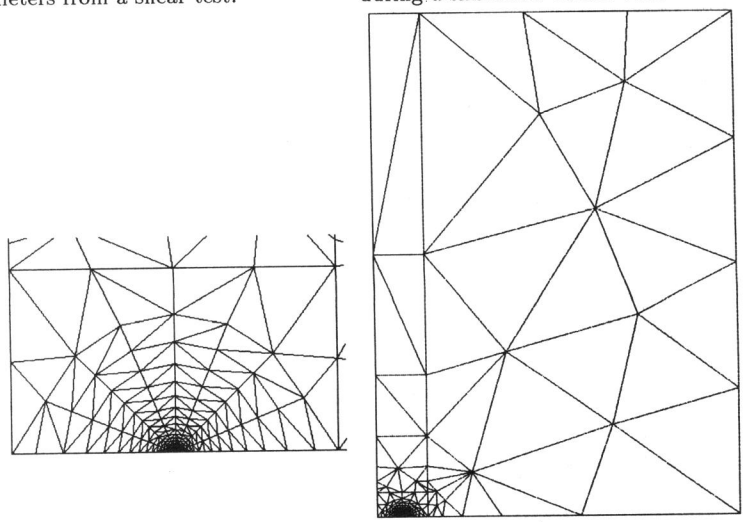

Figure 3: Pre-cracked rectangular body, meshed with 695 pentaedrons. On the left hand side, zoom of the area near the crack.

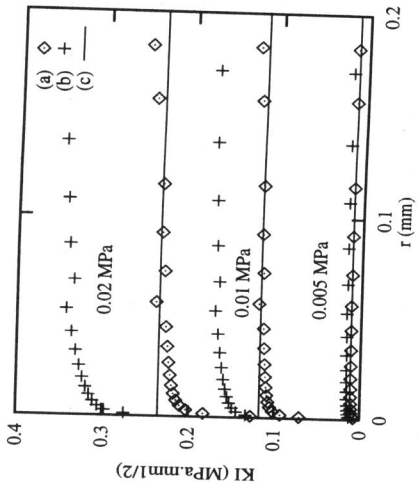

Figure 4: Simulated values of K_I. Comparison with analytical solution.

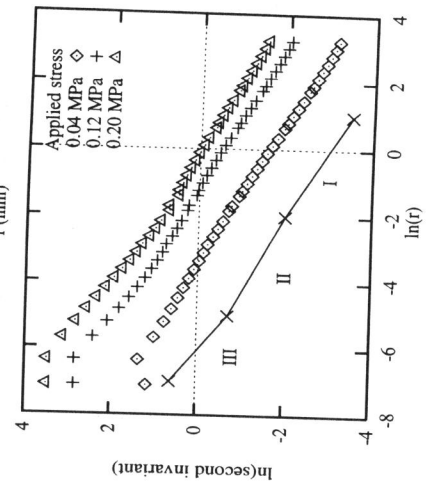

Figure 5: Variation of $\ln(\overline{\Pi}_\sigma^{1/2})$ with $\ln(r)$.

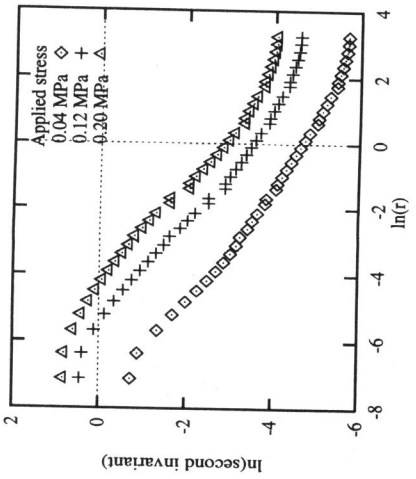

Figure 6: Variation of $\ln(\overline{\Pi}_\varepsilon^{1/2})$ with $\ln(r)$.

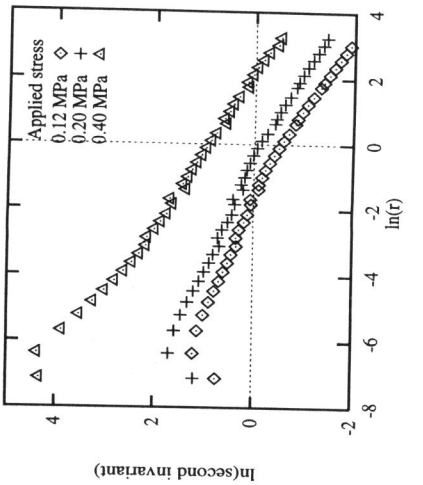

Figure 7: Same as Fig. 5 with $\mu_r = 50$ MPa.